The EMBO Journal (2010) 29, 761–769 | © 2010 European Molecular Biology Organization | All Rights Reserved 0261-4189/10
www.embojournal.org

THE EMBO JOURNAL

Eukaryotic ribonucleases P/MRP: the crystal structure of the P3 domain

Anna Perederina, Olga Esakova, Chao Quan, Elena Khanova and Andrey S Krasilnikov*

Department of Biochemistry and Molecular Biology, Pennsylvania State University, University Park, PA, USA

Ribonuclease (RNase) P is a site-specific endoribonuclease found in all kingdoms of life. Typical RNase P consists of a catalytic RNA component and a protein moiety. In the eukaryotes, the RNase P lineage has split into two, giving rise to a closely related enzyme, RNase MRP, which has similar components but has evolved to have different specificities. The eukaryotic RNases P/MRP have acquired an essential helix-loop-helix protein-binding RNA domain P3 that has an important function in eukaryotic enzymes and distinguishes them from bacterial and archaeal RNases P. Here, we present a crystal structure of the P3 RNA domain from *Saccharomyces cerevisiae* RNase MRP in a complex with RNase P/MRP proteins Pop6 and Pop7 solved to 2.7 Å. The structure suggests similar structural organization of the P3 RNA domains in RNases P/MRP and possible functions of the P3 domains and proteins bound to them in the stabilization of the holoenzymes' structures as well as in interactions with substrates. It provides the first insight into the structural organization of the eukaryotic enzymes of the RNase P/MRP family.

The EMBO Journal (2010) **29,** 761–769. doi:10.1038/emboj.2009.396; Published online 14 January 2010
Subject Categories: RNA; structural biology
Keywords: ribozymes; RNA–protein interactions; RNase P; RNase MRP; *Saccharomyces cerevisiae*

Introduction

Ribonuclease (RNase) P is a site-specific endoribonuclease involved in the metabolism of various RNA molecules including tRNA and rRNA (Guerrier-Takada *et al*, 1983; Altman and Kirsebom, 1999; Kazantsev and Pace, 2006; Kirsebom, 2007; Coughlin *et al*, 2008) and in transcription (Reiner *et al*, 2006, 2008). RNase P is a universal enzyme found in all three kingdoms of life. With a few exceptions (Walker and Engelke, 2008), RNase P is an RNA-based enzyme consisting of a phylogenetically conserved catalytic RNA component and a protein moiety. The RNA component is capable of performing catalysis *in vitro* by itself, albeit with reduced efficiency; the level of activity of the RNA component alone is dramatically lower for the eukaryotic RNase P than that for the bacterial RNase P (Guerrier-Takada *et al*, 1983; Gopalan, 2007; Kikovska *et al*, 2007). The protein moiety is required for the activity of RNase P *in vivo* (Kirsebom *et al*, 1988; Chamberlain *et al*, 1998; Gossringer *et al*, 2006 and references therein).

Compared with bacterial RNase P, the number of protein components grows significantly in eukaryotic RNase P: whereas the bacterial RNase P has a single protein component, *Saccharomyces cerevisiae* RNase P has nine (Walker and Engelke, 2006). Accordingly, the protein content of RNase P holoenzyme is only about 10% by mass in bacteria, but about 75% or more in eukaryotes.

RNase P is evolutionarily related to another RNA-based enzyme, RNase MRP (Chang and Clayton, 1987; Karwan *et al*, 1991). RNase MRP is an endoribonuclease found in practically all eukaryotes analysed (Piccinelli *et al*, 2005). RNase MRP closely resembles eukaryotic RNase P, but has evolved to have different specificity. RNase MRP mostly resides in the nucleolus (Kiss and Filipowicz, 1992) where it is involved in the maturation of rRNA (Schmitt and Clayton, 1993; Henry *et al*, 1994; Lygerou *et al*, 1996; Lindahl *et al*, 2009). RNase MRP was also implicated in the degradation of mRNA involved in the regulation of the cell cycle in yeast (Gill *et al*, 2004). Similar to RNase P, RNase MRP is essential for the survival of the cell. Mutations in the RNA component of human RNase MRP cause the severe autosomal multisystemic disorder cartilage hair hypoplasia (Ridanpaa *et al*, 2001).

The RNA components of RNase MRP and RNase P have multiple common secondary structure features (Figure 1A and B) and share most of their protein components: eight of the nine *S. cerevisiae* RNase P proteins are also found in RNase MRP (Chamberlain *et al*, 1998). All protein components of RNases P/MRP are essential for the survival of the cell (Schmitt and Clayton, 1994; Chamberlain *et al*, 1998; Salinas *et al*, 2005).

The transition from the RNA-rich bacterial to the more complex protein-rich eukaryotic enzymes of the RNase P/MRP family was accompanied by the appearance of a new essential and highly conserved RNA element: a helix-loop-helix P3 RNA domain (Lindahl *et al*, 2000; Ziehler *et al*, 2001; Li *et al*, 2002). The P3 RNA domain is a universal characteristic feature of eukaryotic RNases P/MRP (Piccinelli *et al*, 2005). P3 RNA domains of RNase P and RNase MRP from the same organism closely resemble each other, share sequence elements and are shown to be interchangeable (Lindahl *et al*, 2000; Ziehler *et al*, 2001). P3 is a protein-binding domain, which is crucial for the assembly and maturation of the enzymes; it is suggested to act as a potential nucleation center for the assembly of the multi-component protein moiety (Ziehler *et al*, 2001). The P3 domain is responsible for intracellular localization (Jacobson *et al*, 1995). The P3 RNA domain is involved in direct specific interactions with the RNase P/MRP protein

*Corresponding author. Department of Biochemistry and Molecular Biology, Pennsylvania State University, 106 Althouse Laboratory, University Park, PA 16802, USA. Tel.: +1 814 865 5050; Fax: +1 814 863 7024; E-mail: ask11@psu.edu

Received: 29 September 2009; accepted: 8 December 2009; published online: 14 January 2010

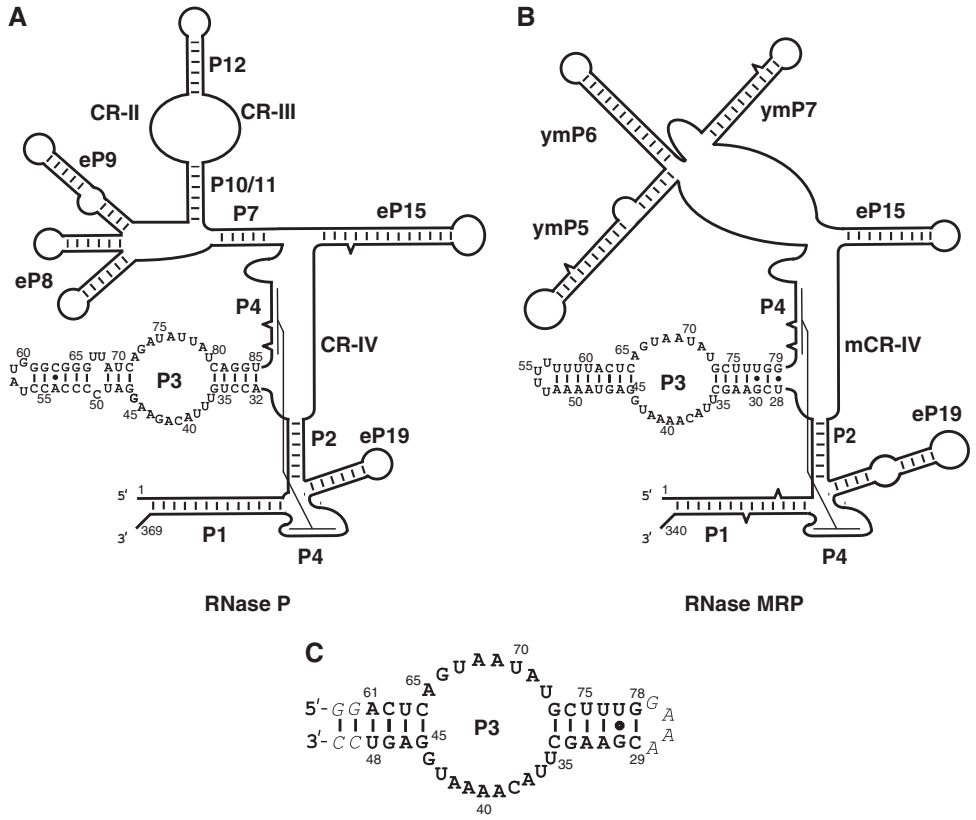

Figure 1 The RNA components of eukaryotic RNase P and RNase MRP have multiple common structural features including the P3 domain. (**A**) Secondary structure diagram of the RNA component of *S. cerevisiae* RNase P. (**B**) Secondary structure diagram of the RNA component of *S. cerevisiae* RNase MRP. (**C**) The modified P3 domain of RNase MRP used in crystallization (the mutated and artificially introduced nucleotides are italicized). The diagrams and the nomenclature of the structural elements are based on Frank *et al* (2000); Li *et al* (2002); Walker and Avis (2004) and Esakova *et al* (2008).

components Pop6 and Pop7 (Pluk *et al*, 1999; Perederina *et al*, 2007; Welting *et al*, 2007) and, possibly, with the protein component Pop1 (Ziehler *et al*, 2001). Certain mutations in the P3 RNA domain affect the assembly of the protein moiety and are detrimental or lethal in yeast (Shadel *et al*, 2000; Ziehler *et al*, 2001; Li *et al*, 2004; Perederina *et al*, 2007). Mutations found in the P3 RNA domain of human RNase MRP result in cartilage hair hypoplasia (Welting *et al*, 2008). Human Pop7 (also known as Rpp20 (Jarrous *et al*, 1998; Aravind *et al*, 2003)) is reported to have ATPase activity (Li and Altman, 2001).

Here, we describe the crystal structure of the P3 RNA domain from *S. cerevisiae* RNase MRP in a complex with common RNase P/MRP protein components Pop6 and Pop7 at 2.7 Å resolution. This structure suggests roles for the P3 domain in the structure and function of RNase P/MRP and provides the first insight into the structural organization of the eukaryotic enzymes of the RNase P/RNase MRP family.

Results

Overview of the structure

The crystallization construct contained proteins Pop6 (18.2 kDa), Pop7 (15.8 kDa) and a modified P3 domain of the RNA component of RNase MRP (46 nucleotides, Figure 1C). The modification changed only distal parts of the helical stems in the P3 RNA domain and did not affect the regions involved in interaction with Pop6/Pop7. The final model included all P3 RNA nucleotides and all protein residues except for 1–3, 122–128 in Pop6 and 1–13, 105–124 in Pop7, and also included 50 water molecules and 3 zinc ions.

The crystallized RNA–protein complex contains one copy of the P3 RNA domain and one copy of the Pop6/Pop7 protein heterodimer, consistent with the stoichiometry that was previously observed biochemically (Perederina *et al*, 2007).

The proteins Pop6 and Pop7 form a compact globule, which is involved in extensive interactions with the well-structured P3 RNA domain (Figure 2), consistent with the results of footprinting analysis (Esakova *et al*, 2008). The formation of the Pop6/Pop7 heterodimer buries 1760 $Å^2$ of the proteins' solvent accessible area, whereas the interaction of the heterodimer with the P3 RNA domain buries 900 $Å^2$ and 1830 $Å^2$ in Pop6 and Pop7, respectively.

Despite having divergent sequences, Pop6 and Pop7 have similar βαβαβαββ folds (Figures 2, 3A and B) that differ from the folds of known bacterial or archaeal RNase P proteins (Stams *et al*, 1998; Boomershine *et al*, 2003; Kazantsev *et al*, 2003; Takagi *et al*, 2004; Wilson *et al*, 2006; Honda *et al*, 2008).

RNA structure and RNA–protein interactions

The P3 RNA domain is folded into two nearly coaxial helical stems separated by an internal single-stranded RNA loop comprised of nucleotides 35–44 and 65–72 (Figures 2 and

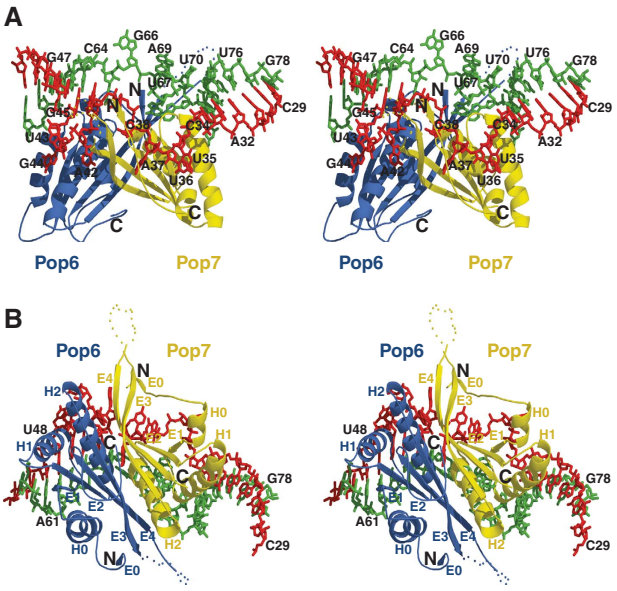

Figure 2 (**A**, **B**) Stereoscopic views of the P3 RNase MRP RNA domain in complex with the RNase MRP/RNase P protein components Pop6 and Pop7. The RNA nucleotides 29–50 are shown in red; nucleotides 59–78 are shown in green; the protein component Pop6 is shown in blue; the protein component Pop7 is shown in yellow; H0, H1, H2-α-helices; E0, E1, E2, E3, E4-β-strands; the positions of the N- and C-terminal ends of the proteins are marked correspondingly. The disordered loops in Pop6 (residues 122–128) and Pop7 (residues 105–124) are symbolized by blue and yellow dots, respectively; the artificially introduced GAAA tetraloop linker connecting the nucleotides 29 and 78 in the crystallization construct is not shown.

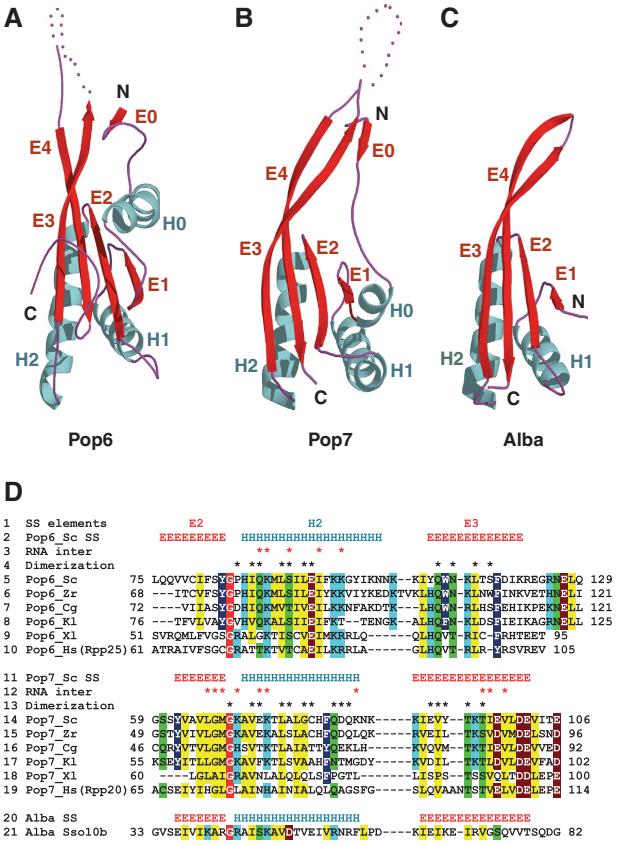

Figure 3 The folds of the RNase P/RNase MRP components Pop6 and Pop7 resemble those found in proteins of the Alba family. H0, H1, H2-α-helices; E0, E1, E2, E3, E4-β-sheets. (**A**) Pop6. (**B**) Pop7. (**C**) *Sulfolobus solfataricus* Alba protein Sso10b (PDB code 1h0x), a typical Alba protein (Wardleworth *et al*, 2002). (**D**) A structure-guided sequence alignment for Pop6 (lines 2–10) and Pop7 (lines 11–19) versus Alba protein Sso10b (lines 20–21). The alignments are shown for *S. cerevisiae* (Sc, lines 5 and 14), *Zygosaccharomyces rouxii* (Zr, lines 6 and 15), *Candida glabrata* (Cg, lines 7 and 16), *Kluyveromyces lactis* (Kl, lines 8 and 17), *Xenopus laevis* (Xl, lines 9 and 18) and human (Hs, lines 10 and 19) proteins. Line 1: secondary structure elements; lines 2, 11 and 20: secondary structures of Pop6, Pop7 and Alba Sso10b (PDB 1h0x), respectively. The residues conserved in Pop6 (lines 5–10), Pop7 (lines 14–19) and Alba proteins (line 21) are highlighted as follows: non-polar aliphatic (GAPVLIM, yellow), aromatic (FYW, dark blue), polar uncharged (STCNQ, green), positively charged (KHR, light blue), negatively charged (DE, brown). The absolutely conserved glycine is highlighted in red. The shown conservation pattern for Alba is based on the alignment of Alba proteins with known structures (PDB ID 1h0x, 1y9x, 1nfj, 1nh9, 2h9u, 2z7c, 2bky, the alignment is not shown). Residues involved in interactions with the P3 domain RNA are marked with asterisks in lines 3 and 12; residues involved in the formation of the Pop6/Pop7 heterodimer are marked with asterisks in lines 4 and 13. For the complete sequence alignment see Supplementary Figure S2.

4A). The structure of the non-helical part of the P3 RNA domain is stabilized mostly by RNA–protein interactions and the stacking of RNA nucleobases: the internal loop of the P3 RNA domain contains no canonical or non-canonical base pairs. The single-stranded RNA section containing nucleotides 35–44 is divided into two distinct segments: because of the stacking of nucleotides G45, A41, A65 and A39 (Figure 4A), the nucleotides A42, U43 and G44 loop out and form a network of interactions with the protein component Pop6; the remaining part of this section is almost exclusively involved in interactions with Pop7 (with the nucleotide A42 being sandwiched between Pop6 and Pop7).

Pop6 and Pop7 are basic proteins (pI 9.28 and 9.34, respectively). The crystal structure reveals that positively charged residues are concentrated mainly in the regions directly involved in interactions with the P3 domain RNA (Figure 5).

The positively charged part of the protein component Pop6 enters the major groove of the distal (left in Figures 1, 2 and 4A) helical stem of the P3 RNA domain in the immediate vicinity of the internal loop. The specificity of the Pop6–RNA interaction comes mostly from the recognition of the looped-out RNA nucleotides A42 and G44 (Figure 4A) as well as from hydrogen bonding between the Hoogsteen edge of nucleotide A39 and the side chain of Gln89 (Figure 4B).

The interaction of the protein component Pop7 with the P3 RNA domain is more extensive than that of Pop6 and involves mostly nucleotides from the single-stranded loop (Figures 2 and 4A). Several nucleotides appear to be of special importance because of the formation of sequence-specific hydrogen bonds with nucleobases: A37 (with Ser20 and Gly67), C38 (with Arg129 and His18), A42 (with Thr96 and Ser132) and U72 (Asn49 and Lys86). The interaction of the nucleotide A37 with Pop7 is especially extensive: A37 actually fills a cavity in the protein (Figure 4C). In addition to their functions in the specificity of RNA–protein interaction, the nucleotides A37, C38 and A39 are an integral part of the Pop7 fold: they are sandwiched between a part of the N-terminal strand of Pop7 (residues 17–24) and the rest of Pop7, thus ordering the N-terminal region of Pop7

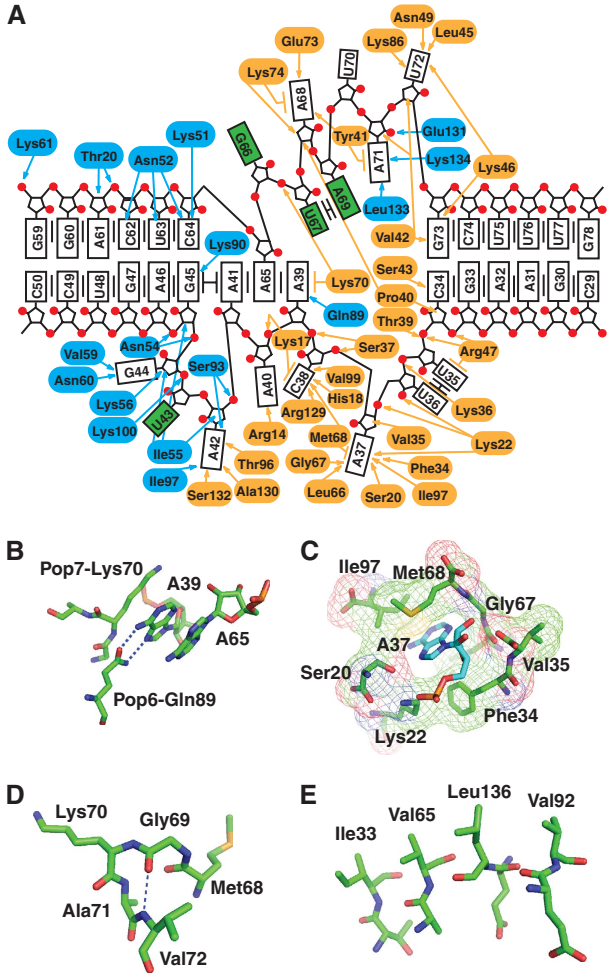

Figure 4 Interactions in the P3 domain. (**A**) RNA–protein interactions. Pop6 residues are highlighted in blue; Pop7 residues are highlighted in orange. P3 domain nucleobases are shown as boxes; P3 loop nucleobases exposed to the solvent are highlighted in green. Van der Waals interactions and hydrogen bonding are shown by arrows; the lines parallel to the nucleobase boxes show stacking interactions. (**B**) Sequence-specific interaction between A39 and Gln89 in Pop6. (**C**) A37 is involved in extensive interactions with Pop7. (**D**) Absolutely conserved Gly69 in Pop7 allows for a sharp turn. (**E**) A stack of hydrophobic residues (Ile33 (β-strand E1), Val65 (β-strand E2), Val92 (β-strand E3) and Leu136 (β-strand E4)) helps stabilize the β-sheet in Pop7.

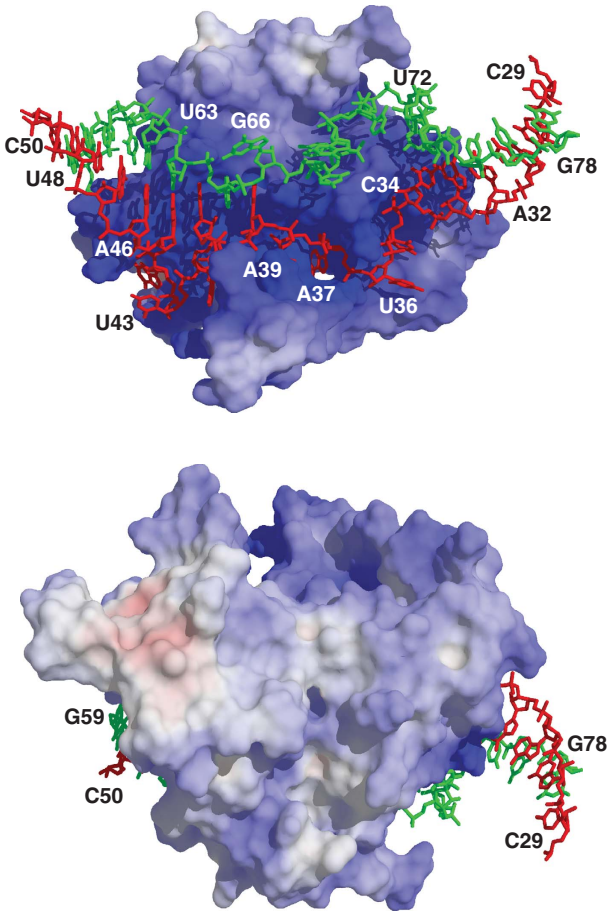

Figure 5 The electrostatic potential of the surface of the Pop6/Pop7 protein heterodimer. The positive charges are located predominantly in the P3 RNA-binding region. Positively charged areas are shown in blue, neutral are shown in white and negatively charged are shown in red. The P3 RNA domain nucleotides 29–50 are shown in red; nucleotides 59–78 are shown in green.

(Figure 2A). These three nucleotides are conserved in a wide range of eukaryotes as an ACR triad (Supplementary Figure S1), suggesting a conserved structural organization of this part of the complex. At the same time, in some cases (such as *Schizosaccharomyces pombe*, Supplementary Figure S1) the ACR triad is absent in P3 RNA domains of RNases P/MRP, possibly indicating an alternative structural organization.

Proteins in the complex

The RNase P/MRP protein component Pop7 (Chamberlain *et al*, 1998) is well conserved in eukaryotes from yeast to vertebrates (Figure 3D; Supplementary Figures S2 and S3). A bioinformatics analysis of Pop7 suggests that Pop7 originates from the Alba family of proteins (Aravind *et al*, 2003). Alba proteins are archaeal and eukaryotic DNA- or RNA-binding proteins involved in RNA metabolism and have the function of a chromosomal protein in some archaea (Aravind *et al*, 2003). Alba proteins form a characteristic βαβαββ fold reminiscent of the folds of DNase I and the C-terminal domain of the translation initiation factor IF_3 (Wardleworth *et al*, 2002) (Figure 3C). Consistent with the results of the bioinformatics analysis, the structure reveals that the core of the Pop7 (α-helices H1, H2 and β-strands E1–E4) folds in a manner resembling the Alba fold (Figure 3B). The positioning of the additional N-terminal β-strand E0 and α-helix H0 is stabilized through their interactions with the P3 domain RNA nucleotides A37, C38 and A39 (Figure 2A).

The pattern of phylogenetic conservation of the Pop7 residues reflects both the general sequence requirements of the Alba fold and the unique requirements imposed by RNA–protein interactions in the Pop7-P3 RNA domain complex (Figure 3D; Supplementary Figures S2 and S3). The most striking example of a feature conserved in all Alba proteins is a glycine residue positioned in the junction between the β-strand E2 and the α-helix H2 (Gly69 in Pop7, Figure 3D). The Alba fold requires a sharp (nearly 180°) turn at this short junction and, apparently, the presence of this absolutely conserved glycine allows for the necessary structural flexibility (Figure 4D). Another example of a structural feature found in Pop7 and conserved in Alba is a stack of

hydrophobic residues Ile33, Val65, Leu136 and Val92 (Figure 4E) that helps stabilize the four-stranded parallel/antiparallel β-sheet (Figure 3B).

Two zinc-binding sites were found to be associated with Pop7 in the crystal structure. One zinc ion is coordinated by two symmetry-related histidines 18 in Pop7. Although having a function in crystal formation, this zinc ion is unlikely to be of physiological relevance. The second, highly anisotropic zinc-binding site (modelled as two partially occupied zinc sites) is formed due to the close positioning of His26 and His30 in Pop7. The two histidines belong to the short α-helix H0 (Figure 3B); the pair is not well conserved phylogenetically (Supplementary Figure S2), and the importance and physiological relevance of this zinc-binding site are not clear.

The protein component of RNase P/MRP Pop6 (Chamberlain *et al*, 1998) is phylogenetically conserved in eukaryotes, although the conservation is weaker than that found for Pop7 (Figure 3D and Supplementary Figure S2; the apparent human counterpart of Pop6 is Rpp25 (Guerrier-Takada *et al*, 2002; Perederina *et al*, 2007; Welting *et al*, 2007)). The weaker phylogenetic conservation of Pop6 is consistent with its role in the P3 domain structure: while Pop7 is involved in extensive specific interactions with the P3 RNA, Pop6 interacts mostly non-specifically with the major groove of a helical part of the P3 RNA domain.

The sequence of the *S. cerevisiae* protein Pop6 is very divergent from the sequences of Pop7 or Alba (Figure 3D; Supplementary Figure S2). Despite this dissimilarity, the overall fold of Pop6 is found to be similar to the fold of Pop7 and Alba (Figure 3A–C). The similarity of the Pop6 and Alba folds is consistent with the results of the bioinformatics analysis, which suggest that human protein Rpp25, an apparent homologue of yeast Pop6, might be evolutionarily related to the Alba family, originating from a paralogue that diverged from the genuine Alba proteins very early in eukaryotic evolution (Aravind *et al*, 2003).

The sequence similarities between Pop6 and Pop7 are concentrated in the area of the β-strand E2 and α-helix H2 and include the presence of the absolutely conserved glycine in the β-strand/α-helix junction (Figure 3D). Overall, considering the degree of the sequence divergence between Pop6 and Pop7, the structural similarity between the two proteins is striking (Figure 3A and B).

Despite the similar structural organization of Pop6 and Pop7, the two proteins interact with their RNA substrates in different manners, and their divergent sequences apparently reflect this difference. Typical Alba proteins have a well-defined positively charged area, likely to be involved in interactions with their nucleic acid substrates (Supplementary Figure S4A); the location of this area is approximately the same in all Alba proteins with known structures (data not shown). The location of this positively charged area in Pop7 matches the location expected for an Alba protein, although the surface of the strongly charged area is considerably larger in Pop7, reflecting the extensity of the protein's interactions with RNA (Supplementary Figure S4B). At the same time, the surface charge distribution in Pop6 is very different (Supplementary Figure S4C), marking a different mode of interaction with RNA. The requirement for a different surface charge distribution apparently results in the divergent sequences, whereas the overall structural organization of the proteins remains remarkably similar.

The formation of the Pop6/Pop7 heterodimer is essential for the interaction with RNA in yeast (Perederina *et al*, 2007); similar results have been obtained for the human proteins (Welting *et al*, 2007). The residues involved in the formation of the heterodimer tend to be phylogenetically conserved (Figure 3D; Supplementary Figure S2), suggesting that Pop6 and Pop7 form a similar heterodimer in RNases P/MRP throughout eukarya. It should be noted that Alba proteins have a propensity to form dimers with a particular juxtaposition of the proteins, and the mutual orientation of Pop6 and Pop7 in the heterodimer resembles that found in Alba dimers (data not shown).

Discussion

Comparison of the P3 domains in RNase P and RNase MRP

The P3 RNA domains from RNases P and MRP have clear similarities in their sequences (Figure 1A and B; Supplementary Figure S1), interact with the same proteins (Perederina *et al*, 2007; Welting *et al*, 2007) and are interchangeable (Lindahl *et al*, 2000). This suggests a very similar structural organization of this part in the two enzymes. The structure of the P3 domain from RNase MRP supports this hypothesis by showing how sequence differences in the P3 RNA domain of RNases P and MRP can be accommodated without causing substantial changes in the structural organization of the domains.

The RNase MRP nucleotides involved in sequence-specific interactions with Pop6/Pop7 appear to be preserved in RNase P (Figure 1A and B; Supplementary Figure S5): the A37, C38, A39 triad (A40, C41, A42 in RNase P), A42 (A45 in RNase P) and U72 (U80 in RNase P). RNase MRP nucleotides U67, A68 and A69 are replaced with A74, U75, A76 and U77 in RNase P; the nucleotides U35 and U36 are replaced with U37, U38 and U39 in RNase P, whereas U43 is missing in RNase P (Supplementary Figure S5). All these deletions and additions are in bulged out segments of the P3 loop (Figures 2A and 4A) and thus might be accommodated without causing significant changes in the RNA fold or RNA–protein interactions, consistent with available results of mutational studies (Ziehler *et al*, 2001).

RNase P has a small internal loop located in the distal (left, Figure 1A) helical stem of the P3 RNA domain (U67, U68), which is not phylogenetically conserved and is not found in RNase MRP (Supplementary Figure S1). Assuming that the position of the loop corresponds to the position of nucleotides A61 and C62 in RNase MRP (Figure 1A and B), this loop is in the immediate vicinity of Ser19 and Thr20 in Pop6 and may serve to strengthen RNA–protein interactions in *S. cerevisiae* RNase P. This hypothesis is consistent with the results of RNase P holoenzyme footprinting, which suggests the involvement of this small internal loop in interactions with proteins (Esakova *et al*, 2008).

P3 domain in RNase P/MRP holoenzymes

Footprinting studies performed on RNase P and RNase MRP holoenzymes show that the P3 RNA domain is involved in extensive interactions with the protein moiety (Esakova *et al*, 2008). The results of the holoenzyme footprinting are overall remarkably consistent with the P3 RNA domain-Pop6/Pop7 structure, suggesting that any other holoenzyme components

interacting with the P3 RNA domain will be involved in only very limited interactions with the P3 RNA domain (with the possible exception of the proximal (right in Figure 1A and B) helical stems).

In the non-helical part of the P3 RNA domain (the P3 domain loop), RNA–Pop6/Pop7 interactions are extensive, protecting most of the non-helical part of the P3 RNA domain and leaving only a few nucleotides, mostly from the upper part of the P3 domain loop, exposed to the solvent: U43, G66, U67 and A69 (Figures 2A and 4A). Similarly, holoenzyme footprinting (Esakova *et al*, 2008) showed complete protection of this region except for U43 (which had its phosphate backbone exposed, but the nitrogen N3 protected in the presence of proteins), A65 (phosphate backbone exposed, N1 protected), G66 (completely exposed), U67 (N3 exposed, but protected from RNase A), A68 and A69 (phosphate backbones protected, but N1 exposed).

Interaction of the Pop6/Pop7 heterodimer allows us to account for the protection observed in the context of the holoenzyme for all nucleotides in the P3 domain loop except for the protection of the nucleobase in U43. Therefore, in this area, substantial involvement of any other proteins is not required to explain the results of the holoenzyme footprinting. On the other hand, this does not exclude interactions of some additional protein component(s) with the P3 domain loop: as most of the nucleotides in the P3 domain loop are not completely buried in the Pop6/Pop7 heterodimer, some of them might have being sandwiched between Pop6/Pop7 and additional protein(s) in the holoenzyme. On the basis of the crystal structure, however, any additional protein interacting with the P3 domain loop would also be expected to be involved in interactions with Pop6/Pop7 and its interaction with the P3 domain loop would not be expected to be extensive.

The results of yeast three-hybrid studies suggest the involvement of Pop1, the largest RNase P/MRP protein component, in specific interactions with the P3 RNA domain (Ziehler *et al*, 2001). Yeast two-hybrid studies suggest interactions between Pop1 and both Pop6 and Pop7 (Houser-Scott *et al*, 2002). Combined, this makes Pop1 a good candidate for the function of an additional protein interacting with the P3 domain loop (likely with the upper part of the P3 domain loop, which is less involved in interactions with Pop6/Pop7). This putative interaction, however, is not expected to be extensive and is likely to be at least partly mediated by the Pop6/Pop7 heterodimer.

According to footprinting studies (Esakova *et al*, 2008), the proximal (right in Figure 1A and B) helical stem of the P3 RNA domain is completely protected in the holoenzyme. Considering the extent of the protected area, it is not likely that this protection is solely due to the protein-stabilized tertiary RNA structure in the holoenzyme, and thus the involvement of the protein moiety is required to explain the holoenzyme footprinting data. The crystal structure shows that the interactions with the Pop6/Pop7 heterodimer cannot account for the observed protection in this part of the P3 RNA domain, thus implying that additional protein(s) (potentially Pop1) must be interacting with this helical stem in a non-specific manner.

The crystal structure shows that Pop6 interacts with several nucleotides of the distal (left in Figures 1, 2 and 4A) helical stem of the P3 RNA domain (nucleotides 45, 59, 61–64, Figure 4A); however, these interactions do not provide substantial protection of ribose in nucleotides 59, 61–64 (Figure 2A). This is consistent with the results of the Fe-EDTA holoenzyme footprinting, which do not show noticeable protection of ribose in these nucleotides in the presence of proteins (Esakova *et al*, 2008). In addition, the holoenzyme footprinting shows a protection of the riboses in nucleotides G45 and A46 (Esakova *et al*, 2008). Although the protection of nucleotide G45 is consistent with the crystal structure, the protection of nucleotide A46 in the holoenzyme cannot be explained by the observed interactions with the Pop6/Pop7 heterodimer. This discrepancy, as well as the protection of the nucleobase in U43 (above), may indicate an interaction with additional component(s) in the context of the holoenzyme.

Functions for the P3 domain in eukaryotic RNase P/MRP

The results of crosslinking the RNA component of eukaryotic RNase P and its substrate tRNA show that the P3 RNA domain is located in close proximity to the ends of the bound tRNA (Marquez *et al*, 2006). Specifically, *S. pombe* nucleotide C54 (corresponding to approximately G73 in *S. cerevisiae* RNase P or G66 in RNase MRP) is found to crosslink both 5′ and 3′ ends of mature tRNA. It should be noted that in the crystal structure of the P3 domain, RNase MRP nucleotide G66 is completely bulged out into the solvent (Figure 2A). The results of holoenzyme footprinting show that this nucleotide is exposed to the solvent and not affected by the protein moiety, thus indicating that the bulged configuration of G66 and, by inference, of G73 in RNase P, is maintained in the context of the holoenzyme as well. Combined with substrate crosslinking data (Marquez *et al*, 2006), this suggests that this nucleotide is available for direct (not protein mediated) interaction with the substrate in the RNase P holoenzyme.

Crosslinking of the substrate to the protein-free *S. pombe* RNase P RNA (Marquez *et al*, 2006) also reveals the proximity of the ends of the substrate tRNA to the area of the lower part of the P3 domain loop, which corresponds to approximately nucleotides 36–39 in *S. cerevisiae* RNase MRP. On the basis of the crystal structure, this area is the location of the protein component Pop7, which suggests that Pop7 is positioned in the immediate vicinity of the substrate cleavage site, potentially participating in the substrate binding, at least in RNase P.

The functions of the multiple protein components in the eukaryotic RNase P/MRP are not clear. The increased complexity of the protein moiety in the eukaryotic (versus bacterial) enzymes of this family is paralleled by the loss of some RNA elements involved in tertiary interactions serving to stabilize the three-dimensional structures of the enzymes (Krasilnikov *et al*, 2003, 2004; Kazantsev *et al*, 2005; Torres-Larios *et al*, 2005). Taking this into account, it is reasonable to suggest that one of the functions of the proteins in eukaryotic enzymes is to help to stabilize the tertiary fold of the catalytic RNA component by taking the place of the missing RNA elements. Modelling the P3 RNA domain into the available structures of bacterial RNase P RNA (Kazantsev *et al*, 2005; Torres-Larios *et al*, 2005), positions the P3 RNA domain and the Pop6/Pop7 heterodimer in the vicinity of the RNA structural elements that serve to stabilize the tertiary structure in bacterial RNases P, but were lost in eukaryotic enzymes (P18, L15/P16/P17 in *Thermotoga maritima*

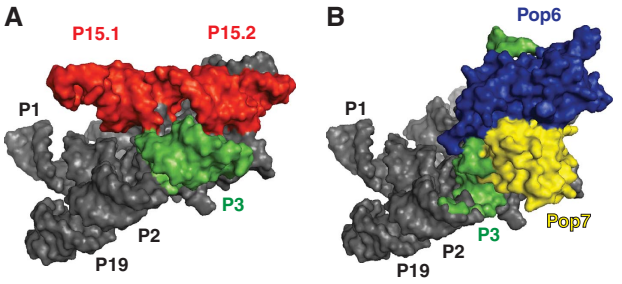

Figure 6 Modelling *S. cerevisiae* RNase MRP P3 RNA domain into the crystal structure of *B. stearothermophilus* RNase P (PDB ID 2A64). The P3 RNA domain and proteins bound to it are positioned in the vicinity of RNA structural elements that serve to stabilize the tertiary fold in bacterial RNase P (Torres-Larios *et al*, 2006), but are missing in eukaryotic enzymes. (**A**) A surface representation of *B. stearothermophilus* RNase P; helical stem P3 is shown in green; stems P15.1 and P15.2 (which stabilize the tertiary structure of bacterial RNase P, but are missing in eukaryotic enzymes) are shown in red. (**B**) A chimerical model built of *B. stearothermophilus* RNase P with stems P15.1, P15.2 removed, and *S. cerevisiae* RNase MRP P3 domain replacing the bacterial P3 stem. Bacterial RNase P is shown in grey; *S. cerevisiae* P3 domain RNA (inserted by superposition of the proximal helical stem of the eukaryotic P3 RNA domain and the bacterial helical stem P3) is shown in green; Pop6 is shown in blue and Pop7 is shown in yellow.

(Torres-Larios *et al*, 2005) and P15.1, P15.2 in *Bacilius stearothermophilus* (Kazantsev *et al*, 2005); Figure 6). This would put the P3 domain and directly or indirectly bound proteins, including Pop6 and Pop7, in a position to replace the lost bacterial RNA elements with protein ones, thus laying the foundation for the evolutionary transition to protein-rich eukaryotic enzymes.

Materials and methods

Crystallization

The Pop6/Pop7 heterodimer was overexpressed in *Escherichia coli* strain BL-21. Cloning, expression and purification of the Pop6/Pop7 heterodimer were described earlier (Perederina *et al*, 2007). Co-expression of Pop6 and Pop7 was required for the solubility of Pop7 (Perederina *et al*, 2007). The modified RNase MRP P3 RNA domain was produced by run-off transcription with T7 RNA polymerase (Milligan *et al*, 1987), followed by purification on 15% denaturing (8 M urea) polyacrylamide gels as described earlier (Perederina *et al*, 2007). The P3 RNA domain–Pop6/Pop7 complexes were produced by incubating the Pop6/Pop7 heterodimer with refolded RNA domain in a 1:1 molar ratio as described by Perederina *et al* (2007). The crystallization was performed in a sitting drop at 19°C under the following conditions: 2 M $(NH_4)_2SO_4$, 200 mM KCl, 5 mM $MgCl_2$, 2 mM $ZnCl_2$, 5% w/v D-trehalose, 2% v/v PEG 400, 100 mM HEPES-Na pH 7.8. The crystals reached their final size of up to $0.65 \times 0.65 \times 0.65$ mm^3 in 1 week. After 1 week, the crystals were transferred into a cryoprotectant solution containing 40% w/v Xylitol, 2 M $(NH_4)_2SO_4$, 200 mM KCl, 5 mM $MgCl_2$, 2 mM $ZnCl_2$, 5% w/v D-trehalose, 2% v/v PEG 400, 100 mM HEPES-Na pH 7.8, then flash cooled and stored in liquid nitrogen. Technical details of the crystallization will be published elsewhere.

Data collection and structure determination

Diffraction data collection was performed at NSLS beamlines X25 and X29A. Both native and initial (wild type) selenomethionine derivative crystals diffracted to about 3.25 Å resolution. Three-wavelength (0.9710 Å, 0.9787 Å and 0.9792 Å) multiple anomalous dispersion data sets for wild-type selenomethionine crystals (space group $P4_222$, unit cell $a = 126.5$ Å, $b = 126.5$ Å, $c = 76.8$ Å, $\alpha = \beta = \gamma = 90°$) were collected. The data sets were integrated and scaled to 3.25 Å resolution using HKL2000 (Otwinowski and Minor, 1997). Initial positions of anomalous scatterers were determined using SOLVE (Brunger *et al*, 1998). The final heavy atom model was refined using SHARP (Fortelle and Bricogne, 1997) and contained 3 Zn ions and 3 Se atoms. The initial phasing information was produced using solvent flattening with Solomon as implemented in SHARP (Fortelle and Bricogne, 1997).

The initial crude model of the complex was built using 3.25 Å-resolution electron density maps obtained for the wild-type selenomethionine derivative crystals. The asymmetric unit contained one molecule of the complex. The initial model contained all RNA nucleotides and most of the amino-acid residues; however, because of the low resolution of the initial electron density maps, the reliable assignment of residues was not possible for some parts of the proteins; the residues that could not be reliably assigned were modelled as alanines, and the initial crude model was not refined further.

To provide additional reference points for the assignment of residues, nine mutants containing one additional methionine in each were produced: Pop6 mutants L115M, T140M and L141M; Pop7 mutants L24M, L52M, L78M, C80M, L100M and L136M. Pop6/Pop7 heterodimers containing these mutants were overexpressed with selenomethionine substituting for methionine, purified and tested for binding to the P3 RNA domain; all of them were found to bind the P3 RNA domain similarly to the wild-type complexes (data not shown). During subsequent crystallization trials, the complexes containing the Pop6 mutant T140M, Pop7 mutants L78M and C80M failed to crystallize in conditions similar to the original crystallization conditions. The remaining six mutants (Pop6 L115M and L141M; Pop7 L24M, L52M, L100M and L136M)

Table I Data collection and refinement statistics[a]

Data collection	
Space group	$P4_222$
Cell dimensions	
a, *b*, *c* (Å)	126.514, 126.514, 76.766
Resolution (Å)	30–2.70 (2.76–2.70)[b]
R_{merge}	0.057 (0.374)
$I/\sigma I$	38.4 (2.0)
Completeness (%)	92.9 (93.3)
Redundancy	5.0 (2.7)
Phasing and refinement	
Resolution (Å)	30–2.70 (2.77–2.70)
No. of reflections	16 346 (970)
SAD phasing power, acentric	1.15
SAD R-Cullis, acentric	0.768
R_{work}/R_{free} (%)	25.0/26.5 (35.5/33.3)
Number of atoms	
RNA	985
Protein	2049
Ions (Zn)	3
Water	50
B-factors (Å^2)	
RNA	98.6
Protein	86.1
Ions (Zn)	81.9
Water	78.0
Overall FOM (Refmac)	0.784
r.m.s. deviations from ideal	
Bond lengths (Å)	0.006
Bond angles (deg)	1.14
Coordinate error (Å), cross-validated Luzzati plot	0.68

[a]The structure was solved by the single wavelength anomalous dispersion (SAD) approach using a crystal of a selenomethionine derivative; a low-resolution model was used in the first step of solvent flattening as described in Materials and methods.
[b]Values in parentheses are for highest-resolution shell.

crystallized under conditions practically identical to the original. The crystals were harvested using a procedure identical to the one used for the wild-type crystals, and used for data collection at a single wavelength of 0.9791 Å. Surprisingly, although five of the mutants produced crystals that diffracted comparably to the original wild-type crystals, one of the mutants, Pop6 L141M, produced crystals that were consistently better diffracting (2.7 Å resolution); all mutants produced crystals in the same spacegroup as the wild type, and with very similar cell parameters.

The final model was built using data obtained with the better-diffracting (2.7 Å) selenomethionine derivative of the Pop6 L141M mutant using single wavelength anomalous dispersion (SAD) phasing. An additional anomalous scatterer was added to the original (low resolution, wild type) heavy atom model; the final heavy atom model contained 4 Se atoms and 3 Zn ions and was refined using SHARP (Fortelle and Bricogne, 1997). To help resolve the phase ambiguity of the SAD phasing, the initial low-resolution crude model of the complex was used in the first step of the solvent flattening as implemented in SHARP. The resulting electron density maps (Supplementary Figure S6), combined with the anomalous signal from the four ordered selenomethionines allowed reliable tracing and assignment of all RNA nucleotides and all residues except for the residues 1–3, 122–128 in Pop6, and 1–13, 105–124 in Pop7. The positions of the residue 115 in Pop6, and residues 24, 52, 100, 136 in Pop7 that were obtained using the anomalous signal from the remaining five mutants, were consistent with the final model, thus providing further verification of the assigned register. A comparison of the final model with the initial low-resolution (wild type) model and electron density maps did not reveal noticeable differences between the Pop6 L141M mutant and the wild-type protein. It is likely that the improved diffraction of the Pop6 L141M mutant is caused by a more uniform crystal packing: the Pop6 residue 141 is located in a hydrophobic core of the protein in the vicinity of one of the crystal-forming intermolecular contact points.

The final model was built using COOT (Emsley and Cowtan, 2004). The refinement was performed using Refmac5 (Murshudov *et al*, 1997) and CNS1.2 (Brunger *et al*, 1998). The final model was refined to R_{free} 26.5% and R_{work} 25.0% with r.m.s. deviations from the ideal bond lengths and angles of 0.006 Å and 1.14° (Table I). Of the protein residues, 204 residues (91.9%) lay in the most favoured regions of the Ramachandran plot, 17 residues (7.7%) in additional allowed regions, 1 residue (0.5%) in the generously allowed region and none in disallowed regions. Three zinc ions were identified based on the anomalous scattering of Zn and were included into the final model along with 50 water molecules. The surface area calculations were performed using AREAIMOL (Lee and Richards, 1971).

Coordinates

The structure has been deposited in the Protein Data Bank (accession code 3IAB).

Supplementary data

Supplementary data are available at *The EMBO Journal* Online (http://www.embojournal.org).

Acknowledgements

We thank P Bevilacqua, A Mondragon, T Pan, J Reese and M Schmitt for valuable comments and suggestions. We thank the stuff of beamlines X25, X29 (NSLS), N Yennawar and H Yennawar (PSU) for help with data collection. NIH-NCRR shared instrumentation grant S10RR023439 and X-ray core facility at the Huck Institute of the Life Sciences are acknowledged. This work was supported by the US National Institutes of Health grant GM085149 to ASK.

Conflict of interest

The authors declare that they have no conflict of interest.

References

Altman S, Kirsebom L (1999) Ribonuclease P. In *The RNA World*, Gesteland RF, Cech TR, Alkins JF (eds), pp 351–380. Cold Spring Harbor, New York, USA: Cold Spring Harbor Laboratory Press

Aravind L, Iyer LM, Anantharaman V (2003) The two faces of Alba: the evolutionary connection between proteins participating in chromatin structure and RNA metabolism. *Genome Biol* **4:** R64

Boomershine WP, McElroy CA, Tsai HY, Wilson RC, Gopalan V, Foster MP (2003) Structure of Mth11/Mth Rpp29, an essential protein subunit of archaeal and eukaryotic RNase P. *Proc Natl Acad Sci* **100:** 15398–15403

Brunger AT, Adams PD, Clore GM, Delano WL, Gros P, Grosse-Kunstleve RW, Jiang JS, Kuszewski J, Nilges N, Pannu NS, Read RJ, Rice LM, Simonson T, Warren GL (1998) Crystallography and NMR system (CNS): a new software system for macromolecular structure determination. *Acta Cryst D* **54:** 905–921

Chamberlain JR, Lee Y, Lane WS, Engelke DR (1998) Purification and characterization of the nuclear RNase P holoenzyme complex reveals extensive subunit overlap with RNase MRP. *Genes Dev* **12:** 1678–1690

Chang DD, Clayton DA (1987) A novel endoribonuclease cleaves at a priming site of mouse mitochondrial DNA replication. *EMBO J* **6:** 409–417

Coughlin DJ, Pleiss JA, Walker SC, Whitworth GB, Engelke DR (2008) Genome-wide search for yeast RNase P substrates reveals role in maturation of intron-encoded box C/D small nucleolar RNAs. *Proc Natl Acad Sci* **105:** 12218–12223

Emsley P, Cowtan K (2004) Coot: model-building tools for molecular graphic. *Acta Cryst D* **60:** 2126–2132

Esakova O, Perederina A, Quan C, Schmitt ME, Krasilnikov AS (2008) Footprinting analysis demonstrates extensive similarity between eukaryotic RNase P and RNase MRP holoenzymes. *RNA* **14:** 1558–1567

Fortelle E, Bricogne G (1997) Maximum likelihood heavy-atom parameter refinement for the multiple isomorphous replacement and multiwavelength anomalous diffraction methods. *Meth Enzymol* **276:** 472–494

Frank DN, Adamidi C, Ehringer MA, Pitulle C, Pace NR (2000) Phylogenetic-comparative analysis of the eukaryal ribonuclease P RNA. *RNA* **6:** 1895–1904

Gill T, Cai T, Aulds J, Wierzbicki S, Schmitt ME (2004) RNase MRP cleaves the CLB2 mRNA to promote cell cycle progression: novel method of mRNA degradation. *Mol Cell Biol* **24:** 945–953

Gopalan V (2007) Uniformity amid diversity in RNase P. *Proc Natl Acad Sci* **104:** 2031–2032

Gossringer M, Far RKK, Hartmann RK (2006) Analysis of RNase P protein (*rnpA*) expression in *Bacillus subtilis* utilizing strains with suppressible *rnpA* expression. *J Bact* **188:** 6816–6823

Guerrier-Takada C, Gardiner K, Marsh T, Pace N, Altman S (1983) The RNA moiety of ribonuclease P is the catalytic subunit of the enzyme. *Cell* **35:** 849–857

Guerrier-Takada C, Eder PS, Gopalan V, Altman S (2002) Purification and characterization of Rpp25, an RNA-binding protein subunit of human ribonuclease P. *RNA* **8:** 290–295

Henry Y, Wood H, Morrissey JP, Petfalski E, Kearsey S, Tollervey D (1994) The 5′ end of yeast 5.8S rRNA is generated by exonucleases from an upstream cleavage site. *EMBO J* **13:** 2452–2463

Honda T, Kakuta Y, Kimura K, Saho J, Kimura M (2008) Structure of an archaeal homolog of the human protein complex Rpp21-Rpp29 that is a key core component for the assembly of active Ribonuclease P. *J Mol Biol* **384:** 652–662

Houser-Scott F, Xiao SH, Millikin CE, Zengel JM, Lindahl L, Engelke DR (2002) Interactions among the protein and RNA subunits of *Saccharomyces cerevisiae* nuclear RNase P. *Proc Natl Acad Sci* **99:** 2684–2689

Jacobson MR, Cao LG, Wang YL, Pederson T (1995) Dynamic localization of RNase MRP RNA in the nucleolus observed by fluorescent RNA cytochemistry in living cells. *J Cell Biol* **131:** 1649–1658

Jarrous N, Eder PS, Guerrier-Takada C, Hoog C, Altman S (1998) Autoantigenic properties of some protein subunits of catalytically active complexes of human Ribonuclease P. *RNA* **4:** 407–417

Karwan R, Bennett JL, Clayton DA (1991) Nuclear RNase MRP processes RNA at multiple discrete sites- interaction with an upstream G-box is required for subsequent downstream cleavages. *Genes Dev* **5:** 1264–1276

Kazantsev AV, Krivenko AA, Harrington DJ, Carter RJ, Holbrook SR, Adams PD, Pace NR (2003) High-resolution structure of RNase P protein from *Thermotoga maritima*. *Proc Natl Acad Sci* **100:** 7497–7502

Kazantsev AV, Krivenko AA, Harrington DJ, Holbrook SR, Adams PD, Pace NR (2005) Crystal structure of a bacterial Ribonuclease P RNA. *Proc Natl Acad Sci* **102:** 13392–13397

Kazantsev AV, Pace NR (2006) Bacterial RNase P: a new view of an ancient enzyme. *Nat Rev Microbiol* **4:** 729–740

Kikovska E, Svard SG, Kirsebom LA (2007) Eukaryotic RNase P RNA mediates cleavage in the absence of protein. *Proc Natl Acad Sci* **104:** 2062–2067

Kirsebom LA, Baer MF, Altman S (1988) Differential effects of mutations in the protein and RNA moieties of RNase P on the efficiency of suppression by various tRNA suppressors. *J Mol Biol* **204:** 879–888

Kirsebom LA (2007) RNase P RNA mediated cleavage: substrate recognition and catalysis. *Biochimie* **89:** 1183–1194

Kiss T, Filipowicz W (1992) Evidence against a mitochondrial location of the 7–2/MRP RNA in mammalian cells. *Cell* **70:** 11–16

Krasilnikov AS, Yang XJ, Pan T, Mondragon A (2003) Crystal structure of the specificity domain of Ribonuclease P. *Nature* **421:** 760–764

Krasilnikov AS, Xiao YH, Pan T, Mondragon A (2004) Basis for structural diversity in homologous RNAs. *Science* **306:** 104–107

Lee B, Richards FM (1971) The interpretation of protein structures: estimation of static accessibility. *J Mol Biol* **55:** 379–400

Li X, Frank DN, Pace NR, Zengel JM, Lindahl L (2002) Phylogenetic analysis of the structure of RNase MRP in yeast. *RNA* **8:** 740–751

Li X, Zaman S, Langdon Y, Zengel JM, Lindahl L (2004) Identification of a functional core in the RNA component of RNase MRP of budding yeasts. *Nucleic Acids Res* **32:** 3703–3711

Li Y, Altman S (2001) A subunit of human nuclear RNase P has ATPase activity. *Proc Natl Acad Sci* **98:** 441–444

Lindahl L, Fretz S, Epps N, Zengel JM (2000) Functional equivalence of hairpins in the RNA subunits of RNase MRP and RNase P in *Saccharomyces cerevisiae*. *RNA* **6:** 653–658

Lindahl L, Bommankanti A, Li X, Hayden L, Jones A, Khan M, Oni T, Zengel JM (2009) RNase MRP is required for entry of 35S precursor rRNA into the canonical processing pathway. *RNA* **15:** 1407–1416

Lopez MD, Rosenblad MA, Samuelsson T (2009) Conserved and variable domains of RNase MRP RNA. *RNA Biol* **6:** 208–220

Lygerou Z, Allmang C, Tollervey D, Seraphin B (1996) Accurate processing of a eukaryotic precursor ribosomal RNA by Ribonuclease MRP *in vitro*. *Science* **272:** 268–270

Marquez SM, Chen JL, Evans D, Pace NR (2006) Structure and function of eukaryotic Ribonuclease P RNA. *Mol Cell* **24:** 445–456

Milligan JF, Groebe DR, Witherell GW, Uhlenbeck OC (1987) Oligoribonucleotide synthesis using T7 RNA-polymerase and synthetic DNA templates. *Nucleic Acids Res* **15:** 8783–8798

Murshudov GN, Vagin AA, Dodson EJ (1997) Refinement of macromolecular structures by the maximum-likelihood method. *Acta Cryst D* **53:** 240–255

Otwinowski Z, Minor W (1997) Processing of X-ray diffraction data collected in oscillation mode. *Meth Enzymol* **276:** 307–326

Perederina A, Esakova O, Koc H, Schmitt ME, Krasilnikov AS (2007) Specific binding of a Pop6/Pop7 heterodimer to the P3 stem of the yeast RNase MRP and RNase P RNAs. *RNA* **13:** 1648–1655

Piccinelli P, Rosenblad MA, Samuelson T (2005) Identification and analysis of Ribonuclease P and MRP RNA in a broad range of eukaryotes. *Nucleic Acids Res* **33:** 4485–4495

Pluk H, van Eenennaam H, Rutjes SA, Pruijn GJM, van Venrooij WJ (1999) RNA-protein interactions in the human RNase MRP ribonucleoprotein complex. *RNA* **5:** 512–524

Reiner R, Ben-Asouli Y, Krilovetzky I, Jarrous N (2006) A role for the catalytic ribonucleoprotein RNase P in RNA polymerase III transcription. *Genes Dev* **20:** 1621–1635

Reiner R, Krasnov-Yoeli N, Dehtiar Y, Jarrous N (2008) Function and assembly of a chromatin-associated RNase P that is required for efficient transcription by RNA polymerase I. *PLoS One* **3:** e4072

Ridanpaa M, van Eenennaam H, Pelin K, Chadwick R, Johnson C, Yuan B, van Venrooij W, Pruijn G, Salmela R, Rockas S, Makitie O, Kaitila I, de la Chapelle A (2001) Mutations in the RNA component of RNase MRP cause a pleiotropic human disease, cartilage-hair hypoplasia. *Cell* **104:** 195–203

Salinas K, Wierzbicki S, Zhou L, Schmitt ME (2005) Characterization and purification of *Saccharomyces cerevisiae* RNase MRP reveals a new unique protein component. *J Biol Chem* **280:** 11352–11360

Schmitt ME, Clayton DA (1993) Nuclear RNase MRP is required for correct processing of pre-5.8S ribosomal RNA in *Saccharomyces cerevisiae*. *Mol Cell Biol* **13:** 7935–7941

Schmitt ME, Clayton DA (1994) Characterization of a unique protein component of yeast RNase MRP- an RNA-binding protein with a Zinc-cluster domain. *Genes Dev* **8:** 2617–2628

Shadel GS, Buckenmeyer GA, Clayton DA, Schmitt ME (2000) Mutational analysis of the RNA component of Saccharomyces cerevisiae RNase MRP reveals distinct nuclear phenotypes. *Gene* **245:** 175–184

Stams T, Niranjanakumari S, Fierke CA, Christianson DW (1998) Ribonuclease P protein structure: evolutionary origins in the translational apparatus. *Science* **280:** 752–755

Takagi H, Watanabe M, Kakuta Y, Kamachi R, Numata T, Tanaka I, Kimura M (2004) Crystal structure of the Ribonuclease P protein Ph1877p from hyperthermophilic archaeon *Pyrococcus horikoshi* OT3. *Biochem Biophys Res Comm* **319:** 787–794

Torres-Larios A, Swinger KK, Krasilnikov AS, Pan T, Mondragon A (2005) Crystal structure of the RNA component of bacterial Ribonuclease P. *Nature* **437:** 584–587

Torres-Larios A, Swinger KK, Pan T, Mondragon A (2006) Structure of ribonuclease P–a universal ribozyme. *Curr Opin Struct Biol* **16:** 327–335

Tranguch AJ, Engelke DR (1993) Comparative structural analysis of nuclear RNase P RNAs from yeast. *J Biol Chem* **268:** 14045–14053

Walker SC, Avis JM (2004) A conserved element in the yeast RNase MRP RNA subunit can participate in a long-range base-pairing interaction. *J Mol Biol* **341:** 375–388

Walker SC, Engelke DR (2006) Ribonuclease P: the evolution of an ancient RNA enzyme. *Crit Rev Biochem Mol Biol* **41:** 77–102

Walker SC, Engelke DR (2008) A protein-only RNase P in human mitochondria. *Cell* **135:** 412–414

Wardleworth BN, Russel RJM, Bell SD, Taylor GL, White MF (2002) Structure of Alba: an archaeal chromatin protein modulated by acetylation. *EMBO J* **21:** 4654–4662

Welting TJM, Peters FMA, Hensen SMM, van Doorn NL, Kikkert BJ, Raats JMH, van Venrooij WJ, Pruijn GJM (2007) Heterodimerization regulates RNase MRP/RNase P association, localization, and expression of Rpp20 and Rpp25. *RNA* **13:** 65–75

Welting TJM, Mattijssen S, Peters FMA, van Doorn NL, Dekkers L, van Venrooij WJ, Heus HA, Bonafe L, Pruijn GJM (2008) Cartilage-hair hypoplasia-associated mutations in the RNase MRP P3 domain affect RNA folding and ribonucleoprotein assembly. *Biochem Biophys Acta* **1783:** 455–466

Wilson RC, Bohlen CJ, Foster MP, Bell CE (2006) Structure of *Pfu* Pop5, an archaeal RNase P protein. *Proc Natl Acad Sci* **103:** 873–878

Ziehler WA, Morris J, Scott FH, Millikin C, Engelke DR (2001) An essential protein-binding domain of nuclear RNase P RNA. *RNA* **7:** 565–575